JOURNAL OF GUIDANCE, CONTROL, AND DYNAMICS
Vol. 29, No. 1, January–February 2006

Endgame Guidance and Relative Navigation of Strategic Interceptors with Delays

Hari B. Hablani*
The Boeing Company, Huntington Beach, California 92803

This paper is concerned with endgame guidance and relative navigation of strategic missiles equipped with divert thrusters to intercept nonmaneuvering reentry vehicles. The paper has three objectives: 1) demonstrate superiority of predictive guidance to pulsed proportional navigation guidance; 2) devise compensation for a one-sample delay in arrival of line-of-sight (LOS) angle measurements at Kalman-filter module and another one-sample delay in communication of LOS rate estimates to the guidance module; and 3) develop a Kalman filter insensitive to modeling errors for relative navigation. A hybrid Kalman filter is developed for relative navigation with angle measurements—hybrid because relative position and velocity vectors are propagated in Cartesian coordinates, whereas the error covariance is propagated, and updated at the time of measurement, in spherical coordinates. For spherical computations, a time-to-go dependent transition matrix and a time-to-go dependent process noise matrix are formulated. It is shown that these time-to-go dependent matrices reduce the miss distance and its sensitivity to modeling errors. With this Kalman filter, it is shown that the closed-loop predictive guidance yields smaller miss distance, consumes less fuel, and requires fewer divert firings than the pulsed proportional navigation guidance does. The delay compensation is accomplished in two steps: first, the high-frequency stream of ΔV measurements from an accelerometer is stored and synchronized with the delayed LOS angle measurement from the seeker; second, the delayed LOS rate estimate from the Kalman filter is propagated forward using the measured ΔV that transpires during the delay. The miss distance of the zero-delay level and robustness to modeling errors is shown to be almost recovered.

I. Introduction

THE objective of this paper is threefold: 1) to show that predictive guidance (also called predicted intercept point or zero-effort-miss guidance) is superior to the proportional navigation guidance in the endgame phase of strategic (exoatmospheric) interceptors using divert thrusters; 2) to demonstrate effectiveness of incremental velocity feed-forward to compensate for the sensor processing and guidance delays and achieve the miss distance that would be achieved in the absence of delays; and 3) develop a relative navigation Kalman filter that achieves a miss distance performance insensitive to modeling errors.

The context of these objectives is as follows. Predictive guidance entails estimation of the closest approach, also called zero-effort-miss (ZEM) distance, of the interceptor to the target in the flight and of the desired transverse incremental velocity to traverse that miss distance in the remaining time to go t_{go}. In contrast with proportional navigation scheme, this guidance scheme is ideally suited for strategic interceptors because they can produce a force of constant magnitude with divert thrusters for a commanded duration and generate the desired incremental velocity. In the absence of sensor or navigation errors, Zarchan[1] shows that, for ballistic engagements wherein the initial distance between the interceptor and a target can be thousands of nautical miles and the flight time to go can be hundreds of seconds, the predictive guidance requires a lower incremental velocity ΔV and, equivalently, less propellant mass than the proportional navigation does. The reason simply is that a lateral ΔV imparted at a time to go t_{go} decreases the miss distance by $(\Delta V)\, t_{go}$, so that the larger the time to go the smaller will be the ΔV to eliminate the zero-effort miss. Of course, proportional navigation can be augmented as in the example of Ref. 1 with gravitational compensation to reduce its ΔV requirement. In contrast with this ballistic engagement scenario, Zarchan concluded from a second example, still in the absence of estimation errors, that the predictive guidance would require more fuel than the proportional navigation if the miss distance were brought to zero in steps by spacing out smaller divert pulses in the flight, instead of one large ΔV in the beginning.[1] These two examples are based on several idealizations: perfect measurements, no guidance or navigation errors besides the initial miss distance, and no sensor or processing delays. It is not known whether, with estimation errors and other realities, the predictive guidance will require more or less fuel than the proportional navigation. The space community, however, has profited from the predictive guidance for several programs: ground-based exoatmospheric/interceptor kinetic kill vehicle, for one, to intercept maneuvering (boosters) and nonmaneuvering targets. So, the first objective of this paper is to show that, in realistic environment of sensor measurement noise, processing delays, divert thruster uncertainties, and relative position, velocity and line-of-sight (LOS) rate estimation errors, the predictive guidance yields smaller miss distances and yet requires less fuel than the proportional navigation guidance does. The scope of this objective in the paper is limited to the endgame phase of the flight, however, unlike the two examples just cited.

Regarding sensor and guidance delays in the homing loop, Zarchan,[1] Ben-Asher and Yaesh,[2] and Shneydor[3] model these delays as a first-order lag or several first-order lags in a series. Optimal guidance laws are developed that compensate for the guidance lag and reduce the acceleration requirements otherwise imposed by the proportional navigation. However, Nesline and Zarchan[4] show that, because of a scale factor or bias error in the estimated time to go $\hat{t}_{go}$, this optimal guidance law lacks robustness and its miss distance is larger than the miss distance with the proportional navigation. Moreover, optimal guidance cannot easily model and analyze the constant acceleration feature of the divert thrusters. On the other hand, strategic interceptor thrusters do not have as much guidance lag as tactical interceptors that use aerodynamic surfaces. The strategic interceptors do have larger sensor and processing delays, however. Franklin et al.[5] furnish a velocity increment feed-forward

Presented as Paper 2000-4272 at the AIAA Guidance, Navigation, and Control Conference, Denver, CO, 14–17 August 2000; received 10 August 2004; revision received 7 April 2005; accepted for publication 6 June 2005.

*Technical Fellow, Engineer/Scientist 6, Flight Sciences and Advanced Designs, Phantom Works. Associate Fellow AIAA.

technique to compensate for the sensor delay and show its effectiveness for satellite attitude control. The second objective of this paper, therefore, is to develop the incremental velocity feed-forward technique for the strategic interceptors and show that this technique can compensate for the sensor and processing delays in the case of interceptors as well.

The third objective of the paper is to develop a Kalman filter for relative navigation, the miss distance performance of which is insensitive to modeling errors. To accomplish this objective, the relative navigation approach devised in the paper is as follows. To estimate relative position and velocity of the target, to estimate zero-effort-miss distance in two lateral orthogonal directions perpendicular to the relative velocity vector, and to estimate the corresponding line-of-sight rates, we will use a hybrid Kalman filter.[6,7] The filter is called *hybrid* because both Cartesian and spherical states are used to minimize the estimation errors.[6–8] The relative position and velocity estimates are propagated in Cartesian coordinates, accounting for the divert acceleration if any in that sample. This eliminates the propagation errors that would arise if the propagation took place in spherical coordinates.[8] At the time of measurement updates, however, because the measurements are bearings (azimuth, elevation) only, the Cartesian state is transformed into a 6×1 spherical state vector and updated using a linear, exact measurement matrix $\underline{H}$ consisting of 0 and 1 and a Kalman gain matrix for the spherical state vector. This eliminates the measurement update errors that would be caused by an extended Kalman filter using partial derivatives of the trigonometric relationships of the LOS angle measurements with the position vector in Cartesian coordinates. The updated spherical state vector is transformed back into a 6×1 Cartesian state vector of relative position and velocity for the next propagation cycle. Mehra[6] and Grossman[7] propagate the error covariance matrix $\underline{P}$ also in Cartesian coordinates and transform it to the spherical coordinates at the time of measurement updates. For simplicity, however, we do not do so; instead, we propagate, as well as update, the error covariance matrix in spherical coordinates using a time-to-go dependent transition matrix and a time-to-go dependent process noise matrix associated with the spherical coordinates. In this study, a range or range rate sensor is not employed, and therefore the simplest spherical state vector for the error covariance matrix and measurement updates to estimate the LOS rates is a 4×1 vector composed of the two LOS angles and their rates. To estimate the relative range and time to go, if desired, the 6×1 spherical state vector mentioned earlier that includes the range r and $\dot{r}$, the corresponding 6×6 spherical transition matrix, and the error covariance matrix can be used. This relative navigation methodology, it will be shown, yields a miss distance performance that is insensitive to modeling errors.

The paper consists of seven sections. Section II presents summarily the line-of-sight angle dynamics and associated transition matrices for error covariance matrix propagation and measurement updates using a hybrid Kalman filter. Section III presents the formulation and architecture of predictive guidance homing loop for strategic interceptors and determination of ZEM threshold and pulse width of the divert thrusters. Section IV presents four homing loops of increasing complexity and realism using pulsed-proportional-navigation (PPN) guidance of exoatmospheric interceptors: 1) the ideal no-delay loop; 2) the loop with one-sample delay caused by the sensor in processing focal plane measurements; 3) the loop with an additional one-sample delay in communication of line-of-sight rate estimate from the hybrid Kalman filter to the guidance module; and finally, 4) the loop of a real strategic interceptor with delay at each module in the loop. The homing loops with delays include compensation for the delays with stored ΔV measurements from the accelerometers and propagating forward the delayed LOS rate estimates using the stored ΔV. Simple formulas are developed for this forward propagation in the guidance module without recourse to the Cartesian propagation in the hybrid Kalman filter. Section V presents process noise matrices for the line-of-sight angles and their rates perturbed by either continuous whitenoise acceleration or discrete random acceleration. These matrices are adaptive for they depend on time to go. Simpler constant matrices are also presented to compare, in Sec. VI, the miss distance performance with time-to-go dependent process noise matrices using predictive or PPN guidance. Superiority of predictive guidance, robustness of miss distance performance attributed to the time-to-go dependent transition matrix and process noise matrix, and the benefits of velocity feed forward in terms of the smallest miss distance are brought forth. Section VII concludes the paper.

II. Transition Matrix Associated with Line-of-Sight Angles and Rates

As stated in the Introduction, the propagation of the true and the estimated relative position and velocity vectors takes place in Cartesian coordinates, but the propagation of the error covariance matrix and the measurement update take place in spherical coordinates. The spherical state vector for the spherical part of the hybrid Kalman filter is usually 4×1, consisting of two LOS angles and their rates. When this work was commissioned, the flight software of the sponsoring interceptor was committed to the 4×1 spherical state vector, and our objective was to improve the miss distance performance without using the 6×1 spherical state vector. We present below both a 4×4 and a 6×6 spherical transition matrix, but the latter is used only to gauge the accuracy of the former, not to replace it.

A. Equations of Motion in Spherical Coordinates

Consider an endgame engagement scenario of an exoatmospheric interceptor on a near-collision course with a target, involving very small azimuth ψ and elevation θ angles (of the order of a few degrees) defined as $\psi = y/x$ and $\theta = -z/x$, where x, y, z are components of the missile-to-target vector in a local inertial frame specified such that the range r subtends the angles ψ and θ with the inertial x axis, and y and z are two perpendicular components much smaller than x (Fig. 1).

For the purposes of guidance, let $a_{\text{div},y}$ and $a_{\text{div},z}$ be the y and z components of the missile divert acceleration in a plane normal to the range r. The LOS angles are, however, so small that $a_{\text{div},y}$ and $a_{\text{div},z}$ are essentially along the inertial y and z axis. It is further assumed that the two vehicles are so close (<25 km) and the remaining time to go is so short (<10 s) that the differential forces (gravitational, atmospheric) between them are negligible and that the target vehicle does not maneuver. Let V_{cl} be the closing velocity of the interceptor. Because of small angles, $\dot{r} = -V_{\text{cl}}$, and $\dot{r}/r \approx -V_{\text{cl}}/(V_{\text{cl}}\ t_{\text{go}}) = -1/t_{\text{go}}$. Under these assumptions, the coupling between azimuth and elevation angles is negligible, and the two angles are governed by the following classical linear, time-varying, uncoupled equations adapted from Ref. 9:

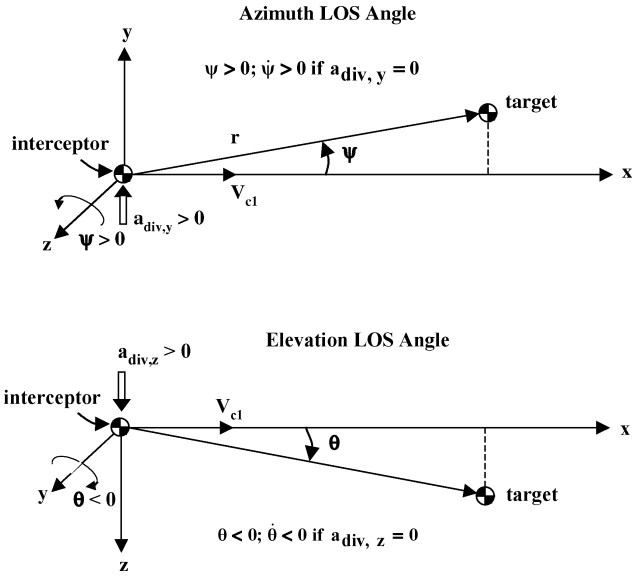

Fig. 1 Opposite signs of LOS angles and their rates for positive miss distances and divert accelerations along the *y* and *z* axes.

y axis: azimuth

$$\ddot{\psi} = (2/t_{go})\dot{\psi} - (1/r)a_{div,y} \tag{1}$$

z axis: elevation

$$\ddot{\theta} = (2/t_{go})\dot{\theta} + (1/r)a_{div,z} \tag{2}$$

These equations govern the lateral (y and z) position and velocity of the target relative to the interceptor, as portrayed in Fig. 1. For the y axis, a positive $a_{div,y}$ acting on the interceptor decreases the positive y separation and the corresponding positive azimuth LOS angle ψ. For the z axis, a positive $a_{div,z}$ decreases the positive z separation and $|\theta|$, where $\theta < 0$.

B. Transition Matrix for a Four-State Spherical Coordinate Vector

To arrive at the transition matrix, these equations are arranged in a first-order form corresponding to the 2×1 states vectors $[\theta \;\; \dot{\theta}]^T$ and $[\psi \;\; \dot{\psi}]^T$. The associated time-varying 2×2 spherical transition matrix $\underline{\Phi}_{2\times 2}(t_{go})$ for each 2×1 state vector, with a sample period $\Delta t \to 0$, is[9]

$$\underline{\Phi}_{2\times 2}(t_{go}) = \begin{bmatrix} 1 & \Delta t \\ 0 & 1 + (2/t_{go})\Delta t \end{bmatrix} \tag{3}$$

Recall that $\underline{\Phi}_{2\times 2}(t_{go})$ is used to propagate the error covariance matrix $\underline{P}$ in spherical coordinates, not to propagate the azimuth and elevation angles themselves. Reflecting on the time-varying term $2\Delta t/t_{go}$ in $\Phi_{2\times 2}(t_{go})$, for $t_{go} = 0.5$ s and $\Delta t = 0.025$ s (40-Hz guidance cycle), $2\Delta t/t_{go} = 0.1$, and for $t_{go} = 0.1$ s, it is 0.5. Thus, as the last few remaining samples are processed, the $2\Delta t/t_{go}$ term becomes significant compared to 1. Because the miss distance in an endgame depends even on the last 10 or so samples before intercept, the time-varying term $2\Delta t/t_{go}$ is important and is retained in the transition matrix.

The time to go is estimated from the Cartesian relative position and velocity of the target estimated by the hybrid Kalman filter. In particular, let $\hat{\underline{r}}$ be the estimate of the true interceptor-to-target position $\underline{r}$ and $\hat{\underline{\dot{r}}}$ be the estimate of the velocity. Though a quick estimate of time to go is $\hat{t}_{go} = |\hat{\underline{r}}|/|\hat{\underline{\dot{r}}}|$, a more accurate estimate is[10,11] $\hat{t}_{go} = -\hat{\underline{r}} \cdot \hat{\underline{\dot{r}}}/\hat{\underline{\dot{r}}} \cdot \hat{\underline{\dot{r}}}$. [In Ref. 10, Abzug defines $\underline{V}_r$ as the interceptor's velocity relative to the target, and therefore $\underline{V}_r = -\underline{\dot{r}} = -(\dot{x}\,\underline{i} + \dot{y}\,\underline{j} + \dot{z}\,\underline{k})$ and not $\underline{V}_r = \underline{\dot{r}}$ as Abzug states. With this correction, Eq. (10), Ref. 10, yields the $\hat{t}_{go}$ just stated.]

Because some error in estimating the t_{go} is likely, a guidance engineer sometimes ignores the t_{go} term in $\underline{\Phi}_{2\times 2}(t_{go})$, presuming that this can be compensated for by tuning the process noise matrix $\underline{Q}$ in the propagation of the error covariance matrix $\underline{P}$. The constant transition matrix $\underline{\Phi}_c$ that follows then is

$$\underline{\Phi}_c = \begin{bmatrix} 1 & \Delta t \\ 0 & 1 \end{bmatrix} \tag{4}$$

which is, incidentally, the exact transition matrix for propagating the relative Cartesian position and velocity in absence of relative gravitational acceleration. In Sec. VI, we will show how seriously this approximation affects the miss distance and renders it sensitive to modeling errors.

Either of the preceding 2×2 transition matrices is used as a diagonal submatrix to construct a 4×4 transition matrix for the 4×1 state vector $[\theta \;\; \dot{\theta} \;\; \psi \;\; \dot{\psi}]^T$.

C. Transition Matrix for a Six-State Spherical Coordinates Vector

It is well known that, depending on the initial estimation errors in $\hat{r}$, $\hat{\dot{r}}$, and $\hat{t}_{go}$, the estimated range and time to go can become negative near intercept, which then cause ill-conditioned computations and degrade the miss distance. Also, to assess the miss distance performance of the 4×4 spherical transition matrices formed from Eqs. (3) and (4) associated with angles and rates only, a six-state transition matrix for the state vector $\underline{x} = [\theta \;\; \dot{\theta} \;\; \psi \;\; \dot{\psi} \;\; r \;\; \dot{r}]^T$ is desired, as it continuously improves the range estimate with angle measurements and divert firings. Whereas the LOS angles are governed by Eqs. (1) and (2), the range r is governed by $\ddot{r} = r(\dot{\psi}^2 + \dot{\theta}^2)$ in the absence of acceleration along r on either vehicle.

A Taylor-series expansion of these equations yields the following 6×6 transition matrix[9] $\underline{\Phi}(t_{go})$:

$$\underline{\Phi}(t_{go}) = \left[\begin{array}{cccc|cc} \multicolumn{4}{c|}{\underline{\Phi}_{2\times 2}(t_{go})} & \multicolumn{2}{c}{\underline{0}} \\ \hline \multicolumn{4}{c|}{\underline{0}} & \multicolumn{2}{c}{\underline{\Phi}_{2\times 2}(t_{go})} \\ \hline 0 & 0 & 0 & 0 & 1 & \Delta t \\ 0 & 2r\dot{\theta}\Delta t & 0 & 2r\dot{\psi}\Delta t & \Delta t(\dot{\psi}^2 + \dot{\theta}^2) & 1 \end{array}\right] \tag{5}$$

which includes two 2×2 transition matrices, Eq. (3), for the angles θ and ψ and their rates, and $\underline{0}$ is a 2×2 null matrix. This matrix agrees with the transition matrix in Ref. 12 if the gravitational acceleration g is taken to be zero and $\dot{r}/r = -t_{go}^{-1}$ is substituted.

III. Predictive and Pulsed-Proportional-Navigation Guidance Laws

Both predictive guidance and PPN guidance can be used for strategic interceptors. The principal difference between the two is in the width of the divert pulses. Although the predictive guidance leads to pulses of variable width—the width can span several guidance cycles or can be shorter than a sample period—the pulse width for proportional navigation is always equal to the sample period or shorter specified a priori.

A. Predictive Guidance

In predictive guidance,[1] one determines the instantaneous zero-effort miss (also called zero control miss[13]) and a corrective ΔV to eliminate that miss distance in the remaining t_{go}. Following Refs. 1 and 14, the ZEM distances along the y and z axes at time to go t_{go} in the absence of any relative acceleration between the two vehicles are given by

$$\mathrm{ZEM}_y = y + \dot{y}t_{go} \tag{6a}$$

$$\mathrm{ZEM}_z = z + \dot{z}t_{go} \tag{6b}$$

These distances are estimated from $\hat{\underline{r}}$ and $\hat{\underline{\dot{r}}}$ furnished by the hybrid Kalman filter after each measurement update in spherical coordinates followed by transformation of the spherical state vector to the Cartesian state vector, and the $\hat{t}_{go}$ estimate is calculated from $\hat{\underline{r}}$ and $\hat{\underline{\dot{r}}}$ as shown earlier.

Because of estimation errors, however, the predictive guidance is designed to nullify a ZEM distance only if the miss estimate is greater than a threshold value $\mathrm{ZEM}_{threshold}$ (see Fig. 2). To develop a relationship between estimation errors and $\mathrm{ZEM}_{threshold}$, recall that ZEM_y and ZEM_z are related to the two orthogonal LOS rates ($\dot{\theta}$ = elevation rate about the y axis, and $\dot{\psi}$ = azimuth rate about the z axis) as follows[1]:

y axis:

$$\mathrm{ZEM}_y = V_{cl}t_{go}^2\dot{\psi} \tag{7a}$$

z axis:

$$\mathrm{ZEM}_z = -V_{cl}t_{go}^2\dot{\theta} \tag{7b}$$

where, for a positive z-miss distance, the elevation rate $\dot{\theta}$ is negative (see Fig. 1). In pulsed proportional navigation, a LOS rate threshold $\omega_{threshold}$ larger than the LOS rate estimation error is introduced, and a divert firing takes place if the estimated LOS rate exceeds that threshold. The corresponding ZEM threshold, according to Eqs. (7), is

$$\mathrm{ZEM}_{threshold} = V_{cl}t_{go}^2\omega_{threshold} \tag{8}$$

which indicates that, for a constant $\omega_{threshold}$, $\mathrm{ZEM}_{threshold}$ varies quadratically with t_{go}. The $\mathrm{ZEM}_{threshold}$ does not decrease to zero, however, as t_{go} approaches zero.[15] Instead, in the presence of estimation error $\delta\omega$ in the LOS rate estimates, δt_{go} in $\hat{t}_{go}$, and δV_{cl} in $\hat{V}_{cl}$, Refs. 15–17 show that $\mathrm{ZEM}_{threshold}$ decreases to a constant nonzero floor value at a certain time to go where, because of the delays and navigation errors, the guidance and navigation system becomes ineffective in reducing the miss distance further (Fig. 2). Denoting

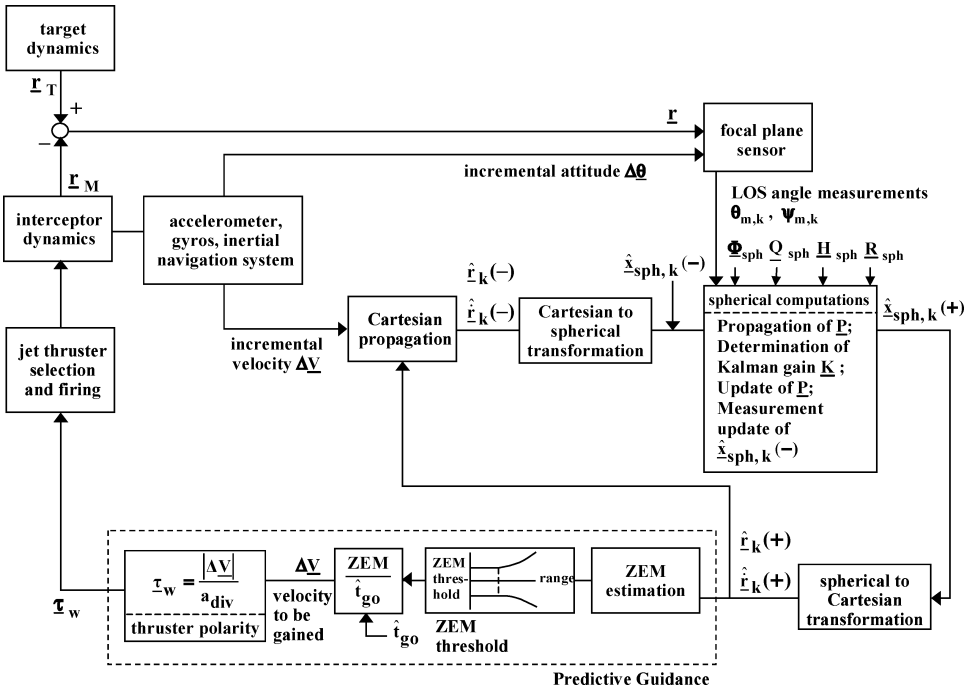

Fig. 2 Predictive guidance homing loop of strategic interceptors using a hybrid Kalman filter.

this time to go as $t_{go,ineff}$ and the corresponding line-of-sight rate as ω_{ineff}, variation of Eq. (8) yields the following minimum value of $ZEM_{threshold}$ (Refs. 16 and 17):

$$ZEM_{threshold} = (\delta\omega)V_{cl}t^2_{go,ineff} + 2\omega_{ineff}V_{cl}t_{go,ineff}(\delta t_{go}) + \omega_{ineff}t^2_{go,ineff}\delta V_{cl} \tag{9}$$

A reasonable value of $t_{go,ineff}$ is twice the total delay in the guidance and navigation loop of the interceptor.[16,17]

To eliminate a ZEM when ZEM_y or ZEM_z exceeds $ZEM_{threshold}$, divert thrusters are fired for a duration that is determined as follows. Let a_{div} be the divert acceleration acting for the duration τ_w, the thrusters being turned on when the time to go is t_{go}. For complete elimination of ZEM in the remaining t_{go}, we have[1]

$$ZEM = \tfrac{1}{2}a_{div}\tau_w^2 + a_{div}\tau_w(t_{go} - \tau_w) \tag{10}$$

where

$$|ZEM| > ZEM_{threshold}, \qquad t_{go} > \tau_w \tag{11a}$$

$$\text{sign}(a_{div}) = \text{sign}(ZEM) \tag{11b}$$

The first term in Eq. (10), quadratic in τ_w, is the distance traveled during the pulse width τ_w, whereas the second term, linear in t_{go}, is the distance traveled in the remaining time $(t_{go} - \tau_w)$ because of the incremental velocity $a_{div}\tau_w$ of the interceptor just imparted by the thrusters.

Denoting $a_{div}\tau_w$ as ΔV, Eq. (10) can be written also as

$$ZEM = (\Delta V)\tau_w/2 + \Delta V(t_{go} - \tau_w) \tag{12}$$

Clearly, if $t_{go} \gg \tau_w$, $ZEM \approx (\Delta V)t_{go}$ and the desired incremental velocity ΔV to eliminate the ZEM linearly over the remaining t_{go} is equal to

$$\Delta V \approx ZEM/t_{go} \tag{13}$$

imparted over the pulse width τ_w equal to

$$\tau_w = \Delta V/a_{div} \qquad \ll t_{go} \tag{14}$$

[Equations (13) and (14) were also derived independently by A. Gianotas, Boeing Company, Anaheim, California.] Equation (13) reveals the benefit of the predictive guidance: the sooner the ZEM is determined without errors, the smaller will be the ΔV needed to null it in the remaining t_{go} and, according to Eq. (14), the shorter will be the pulse width τ_w for a given divert acceleration a_{div}.

Equation (10) can be solved exactly also to yield τ_w equal to

$$\tau_w = t_{go} - \sqrt{t^2_{go} - 2(ZEM/a_{div})} \tag{15}$$

where $\tau_w < t_{go}$. The nondimensional factor $ZEM/(a_{div}t^2_{go}/2)$ that can be formed in the radical in Eq. (15) is the ratio of the ZEM and the lateral distance the interceptor would travel if the divert acceleration a_{div} were to act over the complete remaining t_{go}. Typically, this ratio is much less than unity, and Eq. (15) reduces to the simpler Eqs. (13) and (14). But this ratio could be larger than unity when t_{go} is very small. Equation (15) then does not yield a real τ_w, implying that not enough t_{go} remains to remove all ZEM, and therefore

$$\tau_w = t_{go} \tag{16}$$

In reality, though, because of the delays and navigation errors, the guidance will have to be turned off when $t_{go} = t_{go,ineff}$, as commented earlier.

Figure 2 portrays the closed-loop predictive guidance just developed, using a hybrid Kalman filter for relative navigation. The transformation equations from Cartesian to spherical and conversely are provided in Ref. 18. In Fig. 2, the ZEM and the pulse width $\underline{\tau}_w$ are 2×1 vectors for y and z axis. The vectors $\underline{r}_T$ and $\underline{r}_M$ are the inertial position of the target and the (missile) interceptor, respectively, and $\underline{\hat{x}}_{sph}$ is the estimated 4×1 or 6×1 (depending on the four- or six-state Kalman filter) spherical state vector. The notations $(-)$ and $(+)$ indicate, as usual, the vectors before and after measurement updates. The transition matrix $\underline{\Phi}_{sph}$ is 4×4 or 6×6, made up of two $\Phi_{2\times 2}(t_{go})$ as shown in Eq. (5); $\underline{H}_{sph}$ is the 2×4 or 2×6 measurement matrix, and $\underline{R}_{sph}$ is the 2×2 diagonal measurement noise variance matrix for azimuth and elevation angle measurements. Using gyro-measured attitude of the sensor focal plane, the focal plane measurements are transformed into azimuth and elevation measurements relative to the local inertial frame. The azimuth, elevation, and their rate estimates are updated with measurements; the range r and range rate $\dot{r}$ are updated or not with the measurements depending on whether the estimated spherical state vector is 6×1 or 4×1, respectively.

The guidance loop shown in Fig. 2 is executed at 40 Hz (sample period = 25 ms), but the true equations of motion are integrated, and the pulse width is controlled at 400 Hz (2.5 ms). If the τ_w computed in a cycle is larger than 25 ms, it is recursively replaced with a more current τ_w in the next sample period.

B. Pulsed-Proportional-Navigation Guidance

As stated earlier, in this guidance scheme a divert firing takes place if the estimated LOS rate exceeds the LOS rate threshold $\omega_{\text{threshold}}$; otherwise not. An ω_{thresh} is set according to 1) the expected accuracy of the LOS rate estimate from the Kalman filter, 2) the minimum incremental velocity of the thrusters, and 3) the miss distance specification. Indeed, all of these parameters are interrelated.[15–17] Alternatively, ω_{thresh} can be calculated from the acceleration threshold a_{thresh} equal to a fraction (say, 0.3) of the divert acceleration a_{div}. According to the proportional-navigation guidance law, the commanded acceleration a_{cy} or a_{cz} for y and z axis, respectively, are $a_{cy} = N\hat{V}_{\text{cl}}\dot{\hat{\psi}}$, $a_{cz} = -N\hat{V}_{\text{cl}}\dot{\hat{\theta}}$, where N is the navigation constant, $\dot{\hat{\psi}}$ and $\dot{\hat{\theta}}$ are estimated $\dot{\psi}$ and $\dot{\theta}$, and likewise $\hat{V}_{\text{cl}}$. Divert thrusters are commanded to turn on along the transverse axis y or z if the commanded acceleration a_c exceeds the threshold a_{thresh} for that axis. Because N and V_{cl} are constant, ω_{thresh} corresponding to an a_{thresh} is

$$\omega_{\text{thresh}} = a_{\text{thresh}}/(NV_{\text{cl}}) \tag{17}$$

The LOS rate estimation errors must be less than ω_{thresh} (Refs. 15–17).

The commanded accelerations a_{cy} and a_{cz} do not indicate the desired pulse width of the thrusters, which can only produce the acceleration a_{div}. The commands a_{cy} and a_{cz} could be rewritten, though, as $\Delta V_{cy} = N\hat{V}_{\text{cl}}\Delta\hat{\psi}$ and $\Delta V_{cz} = -N\hat{V}_{\text{cl}}\Delta\hat{\theta}$, where $\Delta\hat{\psi}$ and $\Delta\hat{\theta}$ are the changes in the LOS angles estimated by the Kalman filter over the sample period and ΔV_{cy} and ΔV_{cz} are the desired velocity increments for the next sample. The pulse widths, then, for the y and z axis will be $\tau_{w,y} = |\Delta V_{cy}|/a_{\text{div}}$ and $\tau_{w,z} = |\Delta V_{cz}|/a_{\text{div}}$. One suspects that these time-varying pulse widths will transform pulsed-proportional-navigation guidance into predictive guidance. We will not use these time-varying pulse widths for proportional navigation in this study, however. Instead, the thrusters will be turned on for the entire sample period (25 ms, presently) or for a prespecified fraction thereof (10 ms, presently). As we shall see, when the closest approach is imminent a complete sample period pulse width is too long.

IV. Image Processing Delays and ΔV Feed-Forward Compensation

A. Guidance with No Delays

Figure 3 portrays an ideal, delay-less, discrete guidance, navigation, and control block diagram of a strategic interceptor over one cycle. Though estimated LOS rates and pulsed proportional navigation guidance are explicitly stated in Fig. 3, the following description applies to predictive guidance (Fig. 2) as well, with suitable modifications according to its homing loop. Suppose at time t_{k-1} the divert thrusters are commanded to turn on according to the predictive or pulsed-proportional-navigation guidance policy. Appropriate thrusters then produce acceleration either over a complete sample period $\Delta t = t_k - t_{k-1}$ (25 ms) or over its fraction, depending on the pulse width τ_w. The resulting incremental velocity ΔV_{k-1} is sensed by the accelerometer and communicated to the hybrid Kalman filter. Therein, the Cartesian estimated state vector $[\hat{\underline{r}}^T \quad \hat{\underline{\dot{r}}}^T]$ is propagated from t_{k-1} to t_k according to the equation $\underline{\ddot{r}} = -\underline{a}_{\text{div}}$ in the local inertial frame and transformed to the spherical coordinates. The local inertial LOS angle measurements at time $t = t_k$ are assumed to be available instantly from the focal plane and inertial measurement unit (IMU) for updating the estimated spherical state vector from $\hat{\underline{x}}_k(-)$ to $\hat{\underline{x}}_k(+)$. The updated LOS rate estimates $\dot{\hat{\psi}}_k$ and $\dot{\hat{\theta}}_k$ are then transmitted instantly to the guidance module, and the status of the divert thrusters for the next sample period $t_k \le t \le t_{k+1}$ is determined instantly as well. The thrusters are then turned on/off accordingly at once.

B. Guidance with One-Sample Sensor Delay

The assumption of instantaneous measurement of LOS angles and other instantaneous processes in the homing loop in Fig. 3 is, of course, untenable. The interceptor measures the azimuth and elevation inertial angles of the target with two complementary sensors: a seeker, which measures the location of the target image on the focal plane relative to the focal plane axes, and a gyro, which measures the orientation of the focal plane in an inertial frame.[3,16,19] Although the gyro operates at a very high frequency (400 Hz) and determines vehicle attitude with a negligible delay of 2.5 ms, the seeker performs complex time-dependent electro-optic processes and determines the focal plane measurements in one or two guidance loop samples (each 25 ms long). The seeker thus introduces a significant delay in the focal plane measurements relative to the focal plane attitude measurements from the gyro.

Figure 4 portrays the data flow for the case of a one-sample delay in the LOS angle measurement. The estimated spherical state

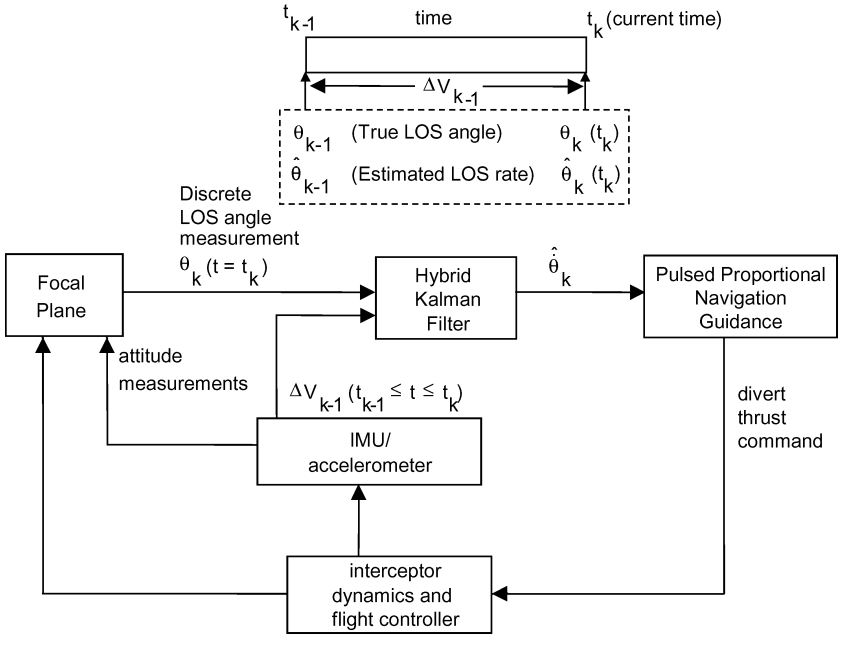

Fig. 3 Pulsed-proportional-navigation guidance homing loop with instantaneous LOS angle measurement and LOS rate estimate (one cycle).

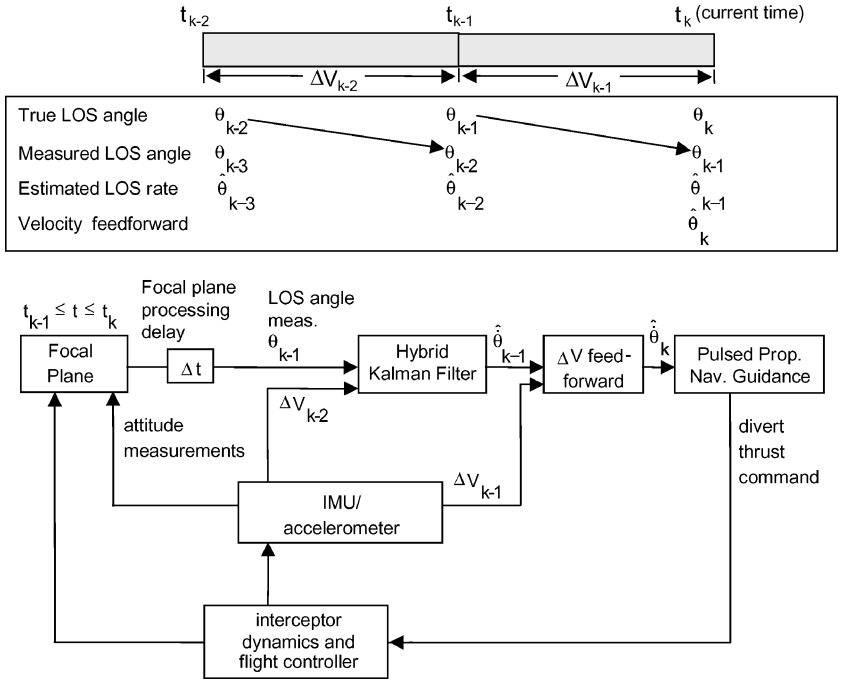

Fig. 4 PPN guidance homing loop with one-sample delayed LOS angle measurement and delta-velocity feed forward (two cycles).

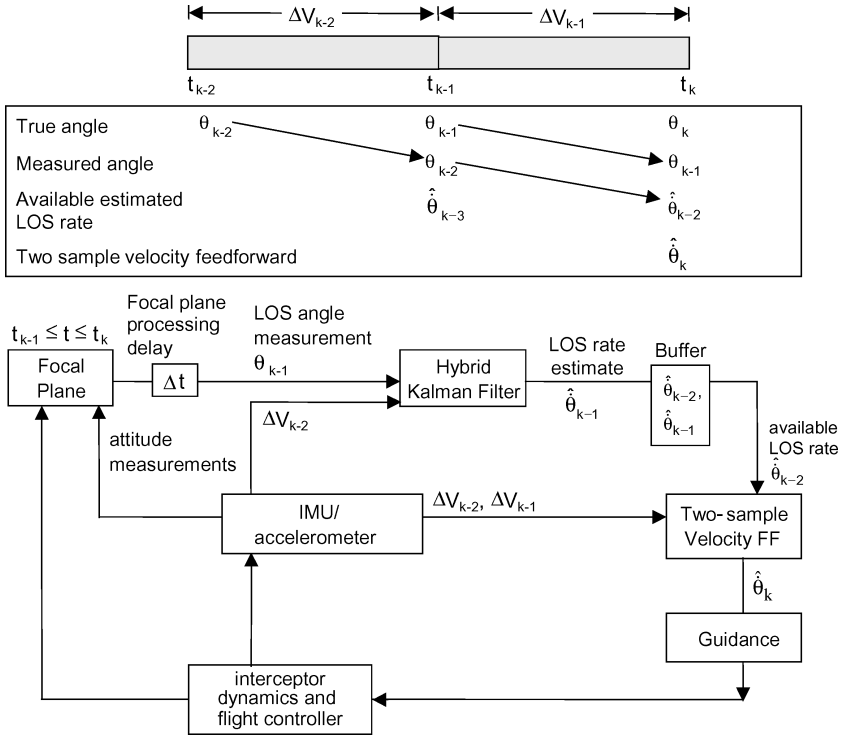

Fig. 5 PPN guidance homing loop with one-sample LOS angle measurement delay, one-sample LOS rate estimate communication delay, and two-sample delta-velocity feed forward of LOS rate estimates (two cycles).

vector $\hat{\underline{x}}_k(-)$ cannot be updated now to $\hat{\underline{x}}_k(+)$ at $t = t_k$ because the contemporaneous azimuth and elevation angle measurements θ_k and ψ_k at $t = t_k$ are not available. Instead, the focal plane, using high-frequency attitude measurements from the gyro in a motion compensation and integration algorithm,[17] provides the measurements $\theta_{k-1}(t_{k-1})$ and $\psi_{k-1}(t_{k-1})$ at $t = t_k$. To use these measurements appropriately, the discrete hybrid Kalman-filter processing is delayed by one sample. As a result, at $t = t_k$ the guidance module receives the one-sample delayed LOS rate estimates $\hat{\theta}_{k-1}$ and $\hat{\psi}_{k-1}$ based on the $\Delta\underline{V}_{k-2}$ during $t_{k-2} \le t \le t_{k-1}$. To compensate for the $\Delta\underline{V}_{k-1}(t_{k-1} \le t \le t_k)$ that might have taken place and has been measured by the accelerometer with a negligible delay of no more than 2.5 ms, the $(k-1)$th LOS rate estimates must be propagated forward by one sample, as shown in Fig. 4. This forward propagation to compensate for the sensor delay is an application of the scheme in Ref. 5, albeit a complicated one because even if $\Delta\underline{V}_{k-1} = 0$, the $(k-1)$th LOS rate estimates must still be propagated forward to account for the changes arising from the change in the target-interceptor range. This $\Delta\underline{V}$ feed-forward of line-of-sight rates is formulated subsequently.

C. Guidance with Two-Sample Sensor and Processing Delays

Next, Fig. 5 illustrates a two-sample delay wherein the hybrid Kalman filter does not furnish the LOS rate estimates $\hat{\theta}_{k-1}$ and

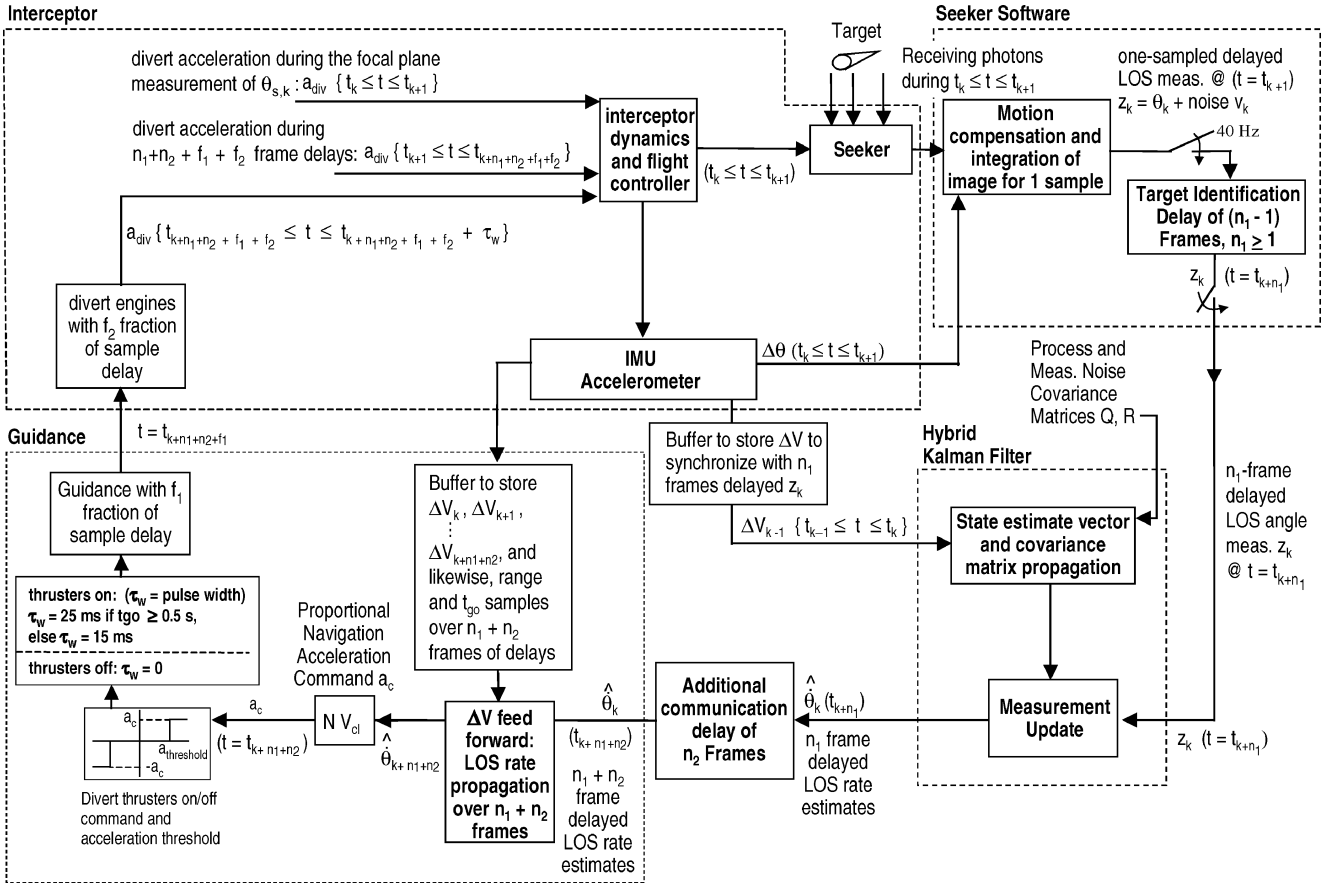

Fig. 6 Homing loop of strategic interceptors with PPN guidance in presence of one-sample image processing delay, $n_1 - 1$ samples of target identification delay, n_2-sample LOS rate estimate communication delay, ΔV feed-forward compensation of $n_1 + n_2$ frames of delay, and uncompensated fractional sample delays of guidance and divert engines; the loop is shown for the cycle $t_{k+n_1+n_2} \le t < t_{k+n_1+n_2+1}$ as influenced by the preceding $n_1 + n_2$ samples.

$\hat{\dot{\psi}}_{k-1}$ spontaneously to the guidance module at $t = t_k$ because the flight computer is occupied performing other higher priority tasks such as target identification, discrimination, and data fusion. As a result, the LOS rate estimates available to the guidance module at $t = t_k$ are two-sample old and must be propagated forward to compensate for the target-interceptor geometry changes during the delay and for $\Delta \underline{V}_{k-2}(t_{k-2} \le t \le t_{k-1})$ and $\Delta \underline{V}_{k-1}(t_{k-1} \le t \le t_k)$.

D. Guidance of a Real Interceptor with Multiple-Sample Delays

Whereas Figs. 3–5 elucidate the data flow simplistically, Fig. 6 portrays a more complete architecture of a single-axis guidance and navigation software of a real exoatmospheric kill vehicle. Starting from the time duration $t_k \le t \le t_{k+1}$ of a guidance sample period, the divert thrust a_{div} dictated by the preceding guidance command acts on the interceptor in this duration. Using motion compensation and integration during $t_k \le t \le t_{k+1}$, aided by the high-frequency attitude measurements from the gyro in this duration, the seeker completes its determination of the focal plane angle measurement $\theta_s(t_k)$ of the target when $t = t_{k+1}$. The local inertial elevation angle θ_k (t_k) is obtained by adding the focal plane angle measurement θ_s (t_k) to a one-sample deliberately delayed and synchronized attitude angle θ_b (t_k) of the focal plane from the IMU, yielding a one-sample delayed, noisy LOS angle measurement z_k at $t = t_{k+1}$: $z_k = \theta_k$ $(t_k) = \theta_b$ $(t_k) + \theta_s$ $(t_k) + \nu_k$, where ν_k consists of diffraction and aberration noise of the seeker and random drift and random walk of the gyro. Additional target identification delays of $n_1 - 1$ sample periods ($n_1 \ge 1$, n_1 is the total number of samples of delay caused by the seeker and target identification) however prevent communication of the measurement $z_k(t_k)$ to the hybrid Kalman filter for measurement update until $t = t_{k+n_1} = t_k + n_1 \Delta t$ (see Fig. 6).

At the end of a sample, the interceptor navigation system provides to the guidance module a cumulative $\Delta \underline{V}$ measurement over the sample period. To bring these measurements in steps with the n_1 frame delayed LOS measurements, the $\Delta \underline{V}$ are stored in a buffer and made available to the hybrid Kalman filter for propagating the estimated spherical state vector from $\hat{\underline{x}}_{k-1}(t_{k-1})$ to $\hat{\underline{x}}_k(-)$ at t_k. At $t = t_{k+n_1}$, the n_1-frame delayed measurement z_k (t_k) is employed to update the estimated spherical state vector from $\hat{\underline{x}}_k(-)$ to $\hat{\underline{x}}_k(+)$. This estimate, however, because of other computational loads of the flight computer, is delayed further by n_2 frames. When the updated LOS rate estimate $\hat{\theta}_k$ finally arrives at the guidance module, the $n_1 + n_2$ increments of $\Delta \underline{V}$ (some $\Delta \underline{V}$ samples can be zero) would have transpired in the interim. Because these $\Delta \underline{V}$ measurements have not been accounted for by the hybrid Kalman filter, the guidance module propagates the estimated LOS rate $\hat{\theta}_k$ from t_k to $t_{k+n_1+n_2}$ using the stored $\Delta \underline{V}$ increments. After feed forward, the LOS rate estimate $\hat{\theta}_{k+n_1+n_2}$ now contemporaneous with the current time $t_{k+n_1+n_2}$ is employed by the guidance scheme, and the on-off status of the divert thrusters for the next sample $t_{k+n_1+n_2} \le t \le t_{k+n_1+n_2+1}$ is determined in accordance with the acceleration threshold a_{thresh}. Negligible fractional sample delays, denoted f_1 and f_2 in Fig. 6, are caused by the computation in the guidance module and on-off transients of the thrusters, but these are much smaller than 25-ms sample period and are disregarded here.

E. LOS Rate Decrement by a ΔV

To determine the LOS rate change caused by a ΔV, consider the elevation angle θ governed by Eq. (2). The change in $\dot{\theta}$ because of the first term on the right-hand side of Eq. (2) arises from the change in the interceptor/target range. This change can be determined in different ways. For instance, from the constancy of $r^2\dot{\theta}$ —the integral of Eq. (2)—equate $r_k^2\dot{\theta}_k$ at $t = t_k$ to $r_{k+1}^2\dot{\theta}_{k+1}$ at $t = t_{k+1}$, where $r_{k+1} = r_k + \dot{r}_k \Delta t$ and $\dot{r}_k / r_k = -l/t_{\text{go},k}$ and apply the binomial theorem to the equation for $\dot{\theta}_{k+1}$. These steps yield the change in $\dot{\theta}_{k+1}$,

which will be shown momentarily. The second term on the right-hand side of Eq. (2) accounts for the change in $\dot{\theta}$ caused by the divert $a_{\text{div},z}$. The guidance cycle operates discretely, with a sample period of Δt, and the navigation furnishes to the guidance module the measurement of ΔV_z over Δt whether the thrusters acted for a complete Δt duration or shorter. Integration of Eq. (2) from t_k to t_{k+1} thus produces the following.

Elevation (z axis):

$$\dot{\theta}_{k+1} \approx \dot{\theta}_k\left(1+\frac{2\Delta t}{t_{\text{go},k}}\right)+\frac{\Delta V_{z,k}}{V_{\text{cl}}t_{\text{go},k}} \tag{18}$$

The first term on the right-hand side of Eq. (18) is also obtained if we use the transition matrix, Eq. (3). Yet another way of deriving Eq. (18) is a simple (Euler) forward integration of Eq. (2). At any rate, in the event of no divert firing Eq. (18) will propagate the LOS rate forward accounting for the interceptor/target range change. The analogous equation for the azimuth LOS rate is as follows.

Azimuth (y axis):

$$\dot{\psi}_{k+1} \approx \dot{\psi}_k\left(1+\frac{2\Delta t}{t_{\text{go},k}}\right)-\frac{\Delta V_{y,k}}{V_{\text{cl}}t_{\text{go},k}} \tag{19}$$

One observes in Eqs. (18) and (19) that the change in the LOS rate by a specified $\Delta V = a_{\text{div}}\tau_w$ is inversely proportional to t_{go}. Therefore, when the closest approach is a few samples away, and so t_{go} is very small, the incremental change in the LOS rate caused by a divert firing could trigger oscillations of the remaining LOS rate and miss distance, each crossing their positive and negative thresholds. To eliminate these oscillations, because a_{div} is constant, τ_w should be narrowed to a smaller value as t_{go} decreases. If mechanized so, the proportional navigation would become similar to the predictive guidance.

Equations (18) and (19) are used recursively to forward the LOS rate estimate over each delay sample period in the guidance module.

V. Process Noise Matrices

To estimate the LOS rates with the hybrid Kalman filter, we must determine and model process noise, measurement noise, and the associated covariance matrices. Although companion papers[16,17] delve into the modeling of seeker and gyro measurement noises, here we only consider modeling the process noise and its covariance matrix. We assume that the process noise stems from uncertainty in the divert thrust magnitude and use statistical properties of the uncertainty derived from the experimental data. This uncertainty also arises from the gyro and accelerometer errors, navigation errors, and target acceleration[20]; not all errors can be modeled as white noise, though.

Consider the motion of the interceptor in the xy plane (azimuth angle ψ, Fig. 1), and let w_ψ (rad/s^2) be a continuous zero-mean white-noise acceleration of azimuth angle ψ. Equation (1) then modifies to

$$\ddot{\psi} = (2/t_{\text{go}})\dot{\psi} - (1/r)a_{\text{div},y} + w_\psi, \qquad w_\psi \sim (0, Q_{\psi\psi}) \tag{20}$$

where $Q_{\psi\psi}$ (rad^2/s^3) is power spectral density of w_ψ. Following the standard process, it can be shown that the associated process noise covariance matrix for propagating the estimation error covariance matrix $\underline{P}$ of the 2×1 state vector $[\psi \;\; \dot{\psi}]^T$ is

$$Q_k(t_{\text{go}}) = Q_{\psi\psi}\begin{bmatrix}\Delta t^3/3 & \Delta t^2/2 + 2\Delta t^3\big/3t_{\text{go}} \\ \text{sym} & \Delta t + 2\Delta t^2\big/t_{\text{go}} + 4\Delta t^3\big/3t_{\text{go}}^2\end{bmatrix} \tag{21}$$

Note that $Q_k(t_{\text{go}})$ is time varying. Observing (modest) complexity of $Q_k(t_{\text{go}})$, it might be tempting to ignore the t_{go} terms because only an estimate of t_{go} is known anyway and the terms involving t_{go} are unimportant until the closest approach is imminent. But the numerical results in Sec. VI show that it is highly beneficial to keep the time-varying $Q_k(t_{\text{go}})$, Eq. (21), as is.

An alternate model of random acceleration is a pulse-to-pulse variation of the divert thrust magnitude, it being constant in a given pulse. Let this random acceleration be denoted as w_{div} (m/s^2), constant in a given sample period $t_{k-1} \le t \le t_k$, but random from sample to sample. Equation (20) is then rewritten as

$$\ddot{\psi} = (2/t_{\text{go}})\dot{\psi} - (1/r)(a_{\text{div},y} + w_{\text{div}}) \tag{22}$$

where $E[w_{\text{div},k}\;\; w_{\text{div},j}] = \sigma^2_{\text{div}}\delta_{jk}$, δ_{jk} is Kronecker delta, and σ^2_{div} has the units of m^2/s^4. Using the average range in a sample period, it can be shown that the covariance matrix associated with the state vector $[\psi \;\; \dot{\psi}]^T$ is

$$Q_k(t_{\text{go}}) = \frac{\sigma^2_{\text{div}}}{r_k^2}\begin{bmatrix}\Delta t^4/4 & (\Delta t^2/2)T_m \\ (\Delta t^2/2)T_m & T_m^2\end{bmatrix} \tag{23}$$

where $T_m = \Delta t + \Delta t^2/t_{\text{go}}$. The acceleration σ_{div} in Eq. (23) can also represent, allegedly,[20] standard deviation of a zero-mean white-noise acceleration of the target.

A beneficial feature of the preceding two process noise covariance matrices is that they both grow with time as t_{go} decreases. As a result, near intercept, the state-space model (the process) used in the hybrid Kalman filter to estimate the LOS rates becomes less important and the measurements more important. Because range is not known accurately, this adaptive feature of $Q_k(t_{\text{go}})$, in line with the comments in Refs. 20 and 21, is a distinct advantage over a time-invariant Q_c used typically in the Kalman filter.

In the Numerical Results section next, the miss distance performance of a guidance scheme with the time-varying $Q_k(t_{\text{go}})$, Eq. (21) or Eq. (23), is compared with that of a time-invariant Q_c obtained by ignoring the t_{go} terms and replacing the time-varying quantity $\sigma^2_{\text{div}}/r_k^2$ with a sort of average, constant σ^2_{av} (units: 1/s^4):

$$Q_c = \sigma^2_{\text{av}}\begin{bmatrix}\Delta t^4/4 & \Delta t^3/2 \\ \Delta t^3/2 & \Delta t^2\end{bmatrix} \tag{24}$$

The 2×2 process noise matrix, Eq. (21), Eq. (23), or Eq. (24) is a block diagonal matrix for $[\theta, \dot{\theta}]^T$ and $[\psi, \dot{\psi}]^T$ in a 4×4 or 6×6 process noise matrix corresponding to a four- or six-element spherical state vector, respectively.

The 2×2 matrix $\underline{Q}$ corresponding to $[r, \dot{r}]^T$ in the six-state spherical state vector excited by a continuous white-noise acceleration with intensity q_r (m^2/s^3) and a discrete white-noise acceleration with variance σ_r^2 (m^2/s^4) are given by, respectively,[21]

$$Q = q_r\begin{bmatrix}\Delta t^3/3 & \Delta t^2/2 \\ \Delta t^2/2 & \Delta t\end{bmatrix} \tag{25a}$$

$$Q = \sigma_r^2\begin{bmatrix}\Delta t^4/4 & \Delta t^3/2 \\ \Delta t^3/2 & \Delta t^2\end{bmatrix} \tag{25b}$$

The results in the next section are based on these process noise matrices.

VI. Numerical Results

A hybrid Kalman filter propagating a 4×4 spherical error covariance matrix along with its measurement update in spherical coordinates is employed in the following illustrations. In the initial stages of the interceptor program that sponsored this study, this filter used the constant transition matrix Φ_c, Eq. (4), instead of $\Phi(t_{\text{go}})$ to estimate the LOS rates, and the hardware-in-the-loop software was developed accordingly. But when the miss distance was found to be sensitive to the delays and process noise matrix, it became imperative to improve its performance and render it insensitive to modeling errors but without including the range and range rate in the spherical state vector so as to minimize the changes in the software. Next, the miss distance performance of the hybrid Kalman filter using a 4×4 spherical error covariance matrix is compared with the performance using a 6×6 spherical error covariance matrix. The estimation error covariance matrix $\underline{P}$, the process noise matrix $\underline{Q}$,

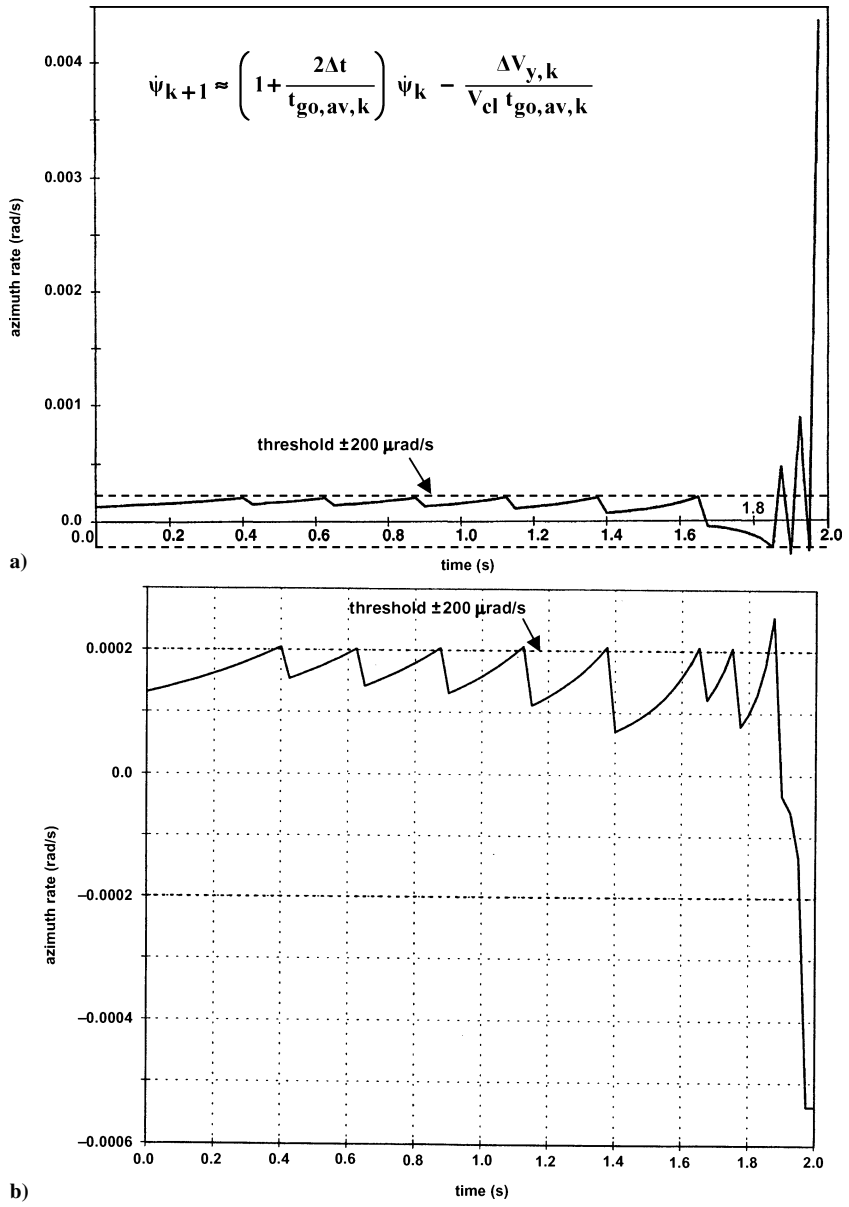

Fig. 7 Oscillations of azimuth LOS rates across thresholds are eliminated by shortening the pulse width: a) 25-ms pulse widths all of the way and b) 25 ms for $t_{go} > 0.5$ s and 10 ms for $t_{go} \leq 0.5$ s.

the measurement matrix $\underline{H}$, the measurement noise covariance matrix $\underline{R}$ for the two LOS angle measurements, and the Kalman gain matrix $\underline{K}$ all correspond to either the four- or six-element spherical state vector. The seeker noise is modeled as white: 20 μrad (1σ) when divert thrusters are off and 50 μrad (1σ) when a divert is on, to reflect a more jittery focal plane at the time of thruster firing. The guidance loop frequency is 40 Hz. The gyro and accelerometer noises are not considered, but because these errors are indeed process noises a fraction of the process noise matrix $\underline{\underline{Q}}$ could be regarded as representing the noise of these instruments.

A. Need for Shorter Pulses as t_{go} Approaches Zero

As stated earlier, the most powerful feature of the predictive guidance is the pulse-width modulation according to the remaining miss distance and time to go. For a given t_{go}, as miss distance decreases, the predictive guidance reduces the pulse width until it is equal to the minimum impulse bit. In proportional navigation guidance, however, the pulse width remains equal to the sample period of the guidance system regardless of t_{go}. The disadvantage of this is that, as observed earlier, the residual LOS rate starts oscillating over the LOS rate threshold channel as t_{go} approaches zero. For a certain engagement scenario under PPN guidance using true LOS rate, Fig. 7a illustrates these progressively larger decrements of azimuth LOS rate with 25-ms divert pulses whenever the LOS rate exceeds $\omega_{threshold} = 200$ μrad/s. As the interceptor approaches the target and t_{go} decreases below 0.4 s, a 25-ms pulse changes the sign of the LOS rate. In view of Eq. (7a), this implies that the corresponding ZEM distance along the local inertial y axis also changes its sign: instead of missing the target from one side, the interceptor will now miss the target from the opposite side. This firing is clearly wasteful, and it prompts repeated unstable firing of the pulses in opposite directions. These opposite firings can be eliminated or delayed considerably by using shorter, say, 10 ms, pulse widths after $t_{go} = 0.5$ s. This is illustrated in Fig. 7b, in which azimuth LOS rate is attenuated without causing oscillations near intercept at $t = 2$ s.

This establishes the need for decreasing the pulse width in the PPN guidance as an interceptor approaches the target, at once improving the miss distance and reducing the fuel consumption. Predictive guidance, however, possesses this feature inherently.

B. Predictive Guidance Using a Constant Transition Matrix Φ_c

It is instructive to compare performance of the closed-loop predictive guidance in Fig. 8 with that of the noise-free predictive guidance in Ref. 1, using a quadratic ZEM threshold equal to $V_{c1} t_{go}^2\, \omega_{thresh}$

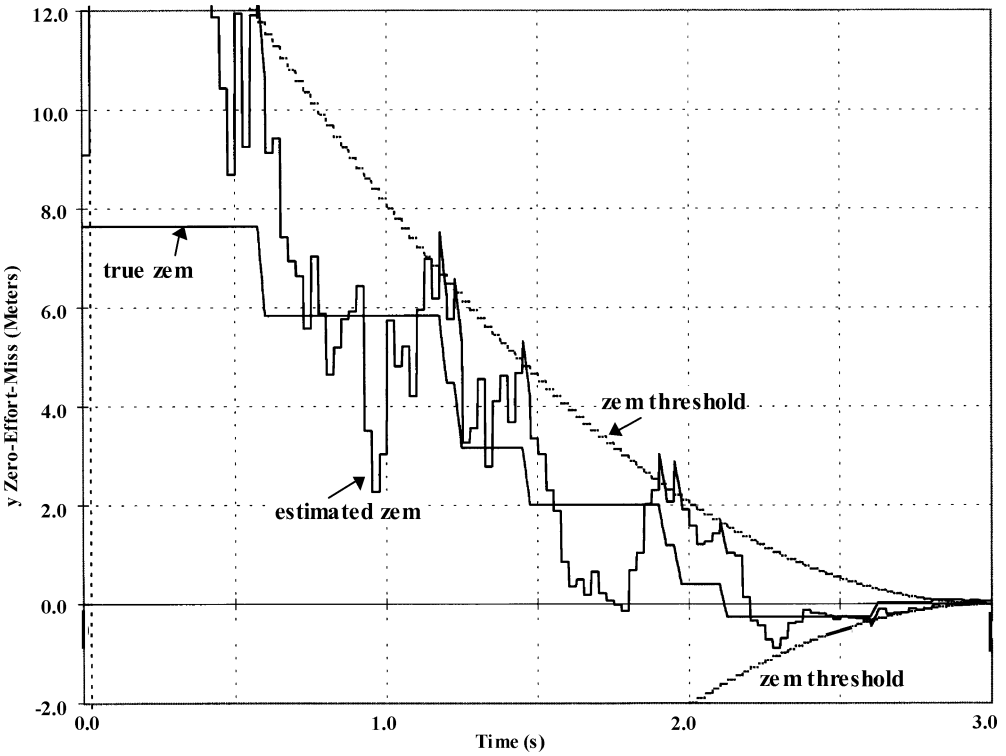

Fig. 8 Performance of predictive guidance using the pulse widths 25 ms $\geq \tau_w \geq$ 10 ms: a four-state constant transition matrix.

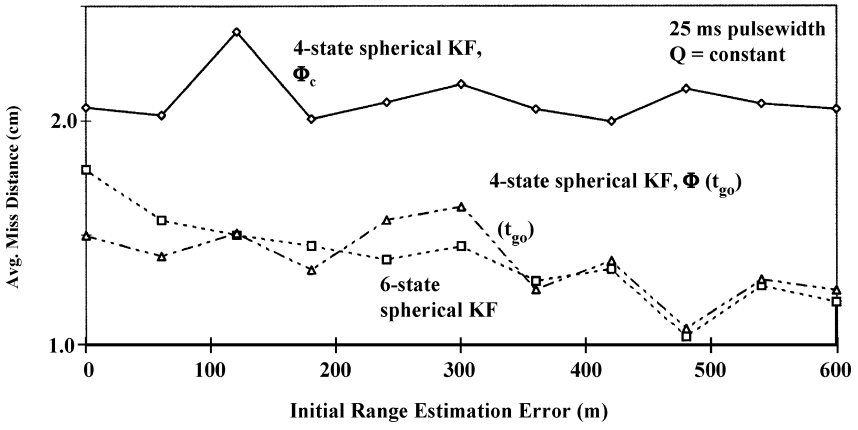

Fig. 9 Time-to-go dependent spherical transition matrices $\Phi(t_{go})$ yield smaller miss distances than the constant transition matrix Φ_c.

(without a constant ZEM near $t_{go} = 0$), a variable pulse width τ_w, 10 ms $\leq \tau_w \leq$ 25 ms, and a constant process noise matrix, Eq. (24). Spherical error covariance matrices are propagated using the constant transition matrix Φ_c, Eq. (4), and updated at the time of LOS angle measurements. The ΔV pulses, not shown here, are 25 ms wide until $t_{go} \leq 0.5$ s, and then they are 17.5, 10, and 12.5 ms (controlled by a 400-Hz integration frequency). In Fig. 8, the intercept occurs at $t = 3$ s, and the thrusters are fired whenever the estimated ZEM exceeds the ZEM threshold. Near $t = 2.1$ s, a divert pulse of 25-ms width pushes the true ZEM to the opposite direction. After $t = 2.5$ s, the narrower pulses control the miss distance to ~10 cm. This closed-loop predictive guidance result is remarkably different from the open-loop deterministic result in Ref. 1.

C. PPN Guidance with 4 × 4 and 6 × 6 Transition Matrices and Adaptive $Q(t_{go})$

We will now show that the t_{go} dependent transition matrix $\Phi(t_{go})$ yields smaller miss distance than the constant transition matrix Φ_c. We present the results of Monte Carlo runs for which the initial estimation error $\tilde{r}_0$ in relative range is varied in steps of 60 m from 600 m to 0 m: 600, 540, 480, . . . , 0 m. The limit 600 m arises from the maximum expected in-flight target update error using global positioning system (GPS). The $\tilde{r}_0$ is such that the corresponding estimated range is greater than the true range, resulting always in a positive $\hat{t}_{go}$; should $\hat{t}_{go}$ become negative, it is rendered positive by stipulating that if $\hat{t}_{go} < 2\Delta t$, then $\hat{t}_{go} = 2\Delta t$. For each $\tilde{r}_0$ error, 50 endgame scenarios are simulated, each 3 s long, using different random seeker noise sequences. Figure 9 compares average miss distance vs $\tilde{r}_0$ for three schemes of error covariance matrix propagation in the hybrid Kalman filter: 1) using the constant 4 × 4 transition matrix Φ_c, 2) using the six-state spherical transition matrix, and 3) using the four-state t_{go} dependent transition matrix $\Phi(t_{go})$. All three schemes use 25-ms pulses and a constant Q_c. For all of the cases, the diagonal elements of the spherical error covariance matrix $\underline{P}$ are initialized to (20 μrad)^2 for azimuth and elevation errors and (20 μrad/0.025 s = 800 μrad/s)^2 for azimuth and elevation rate errors. [The 800-μrad/s line-of-sight rate estimation error initialization is excessive, as we learned later. Kalman filter reduces it to ~100–200 μrad/s (Refs. 16 and 17).] In the case of the six-state transition matrix, the diagonal elements corresponding to the range and range rate errors are equal to the specified $\tilde{r}_0^2$ and zero, respectively.

1. Constant Process Noise Matrix Q_c

The four-state constant transition matrix Φ_c propagates the error covariance matrix $\underline{P}$ progressively less accurately as t_{go} approaches zero. Thus, Φ_c induces an implicit process noise matrix $Q_{implicit}$ in the propagation of $\underline{P}$, and $Q_{implicit}$ grows as the interceptor approaches the target. In contrast, if one uses the 6×6 time-varying transition matrix, Eq. (5), then there is no implicitly growing process noise matrix, and the propagation of the error covariance matrix is proper. Because this 6×6 transition matrix provides progressively more accurate estimate of the range and t_{go} as t_{go} diminishes, the miss distance for the six-state spherical Kalman filter in Fig. 9 is less than the miss distance for the 4×4 constant transition matrix Φ_c. This decrease in the miss distance is attributed to the term $2\Delta t/t_{go}$ in $\Phi(t_{go})$ in Eq. (3). We therefore speculate that if the $4 \times 4 \Phi_c$ is replaced with the $4 \times 4\ \Phi(t_{go})$, the miss distance performance would improve, though the range estimation error will not decrease and the attendant contribution of t_{go} error to the miss distance would persist.[16] This speculation is validated in Fig. 9, where we observe that the $4 \times 4\ \Phi(t_{go})$ indeed achieves a smaller miss distance than the $4 \times 4\ \Phi_c$ and nearly the same miss distances as those by the 6×6 transition matrix $\Phi(t_{go})$.

2. Adaptive Process Noise Matrix $Q(t_{go})$

Figure 10 optimizes $\underline{Q}$ for propagating the 4×4 error covariance matrix by introducing a scalar q such that $\underline{Q} = q\underline{Q}_c$ or $\underline{Q} = q\underline{Q}(t_{go})$ and vary q. Furthermore, unlike heretofore, a random sample-to-sample 5% variation in the divert thrust magnitude is included in the runs, in accordance with Eq. (22). Three different cases are considered: Φ_c with $\underline{Q}_c$, $\Phi(t_{go})$ with $\underline{Q}(t_{go})$, and $\Phi(t_{go})$ with $\underline{Q}_c$. All discrete points on the curves are the averages of the Monte Carlo runs, each Monte Carlo with 100 random runs and each run with a ground-tracking initial relative range estimation error of $\tilde{r}_0 = 2500$ m. For the first case, Φ_c with $\underline{Q}_c$, Fig. 10 shows that the minimum miss distance is equal to ~4 cm at $\sqrt{q} = 2$. The second case, $\Phi(t_{go})$ with $\underline{Q}(t_{go})$, exhibits the same minimum miss distance but at a higher optimum q; $\sqrt{q} = 10$ because of lesser modeling errors. More importantly, though, we also see that the miss distance is now less sensitive to q because the time-varying $\Phi(t_{go})$ and $\underline{Q}(t_{go})$ have lesser modeling errors than the constant Φ_c and $\underline{Q}_c$. Finally, the minimum miss distance for the third case, $\Phi(t_{go})$ with $\underline{Q}_c$, is still the same as in the other two cases, but now it occurs at $\sqrt{q} = 1$ and is the least sensitive of all to $\sqrt{q}$.

From these comparative results, we conclude that one should use $\Phi(t_{go})$ and Q_c with $q = 1$ for propagating the 4×4 spherical error covariance matrix, resulting in a miss distance least sensitive to the modeling errors. That the minimum miss distance is the same for all three cases, ~4 cm, is not intriguing because that is irreducible distance and it depends on common parameters in all runs, namely, sensor noise, pulse width, thrust magnitude, thrust or LOS rate thresholds, and the navigation constant (equal to four here).

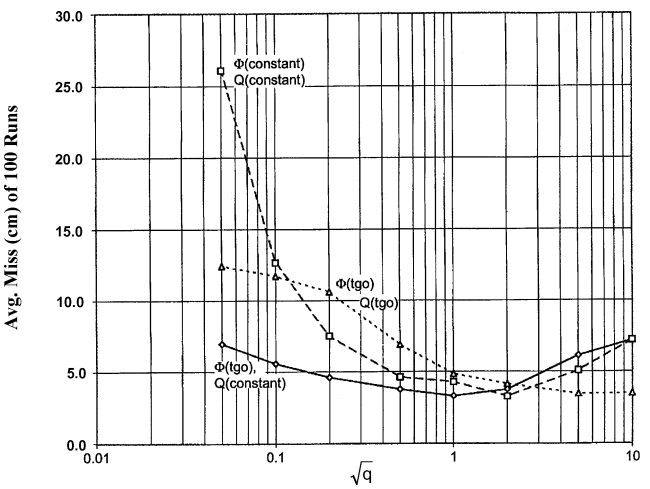

Fig. 10 Influence of time-to-go dependent spherical transition matrix $\Phi(t_{go})$ and process noise matrix $Q(t_{go})$ on miss distance and optimization of $\underline{Q}$: initial range error equal to 2500 m (0.34-s bias error in t_{go}).

D. Predictive vs PPN Guidance

These two guidance laws are compared in Fig. 11 for their miss distance performance and fuel consumption (average total ΔV). Unlike the results in Figs. 9 and 10, the miss distances in Fig. 11 are each an average of 650 runs: 13 initial relative range estimation errors ($\tilde{r}_0 = 600, 550, 500, \ldots, 50, 0$ m) and 50 runs for each $\tilde{r}_0$ with different seeker measurement noise seeds.

1. PPN Guidance

All of the results in Fig. 11 are based on the navigation constant $N = 4$ unless noted otherwise. Figure 11 shows that, using Φ_c for propagating the error covariance matrix, when the pulse width is narrowed from all pulses 25 ms to 25/10 ms (10 ms after $t_{go} \leq 0.5$ s), the average miss distance decreases from 2.1 to 1.7 cm, and the corresponding average cumulative delta velocity (propellant consumption) decreases from 17.2 to 13.2 m/s (see the symbols ♦ labeled PPN and connected by the arrows in the direction of improving performance). With the $6 \times 6\ \Phi(t_{go})$, the miss distance reduces further to 1.2 cm. When the $6 \times 6\ \Phi(t_{go})$ is replaced with the $4 \times 4\ \Phi(t_{go})$, the miss distance reduces to 1.1 cm, similar to the earlier results in Fig. 9. The navigation constant $N = 3$ is known to be optimum in the absence of noise or estimation errors for intercepting a nonmaneuvering reentry vehicle using proportional navigation. The miss distance, ~1.35 cm, in Fig. 11 using the $4 \times 4\ \Phi(t_{go})$ and 25/10-ms pulse is slightly higher for $N = 3$ than for $N = 4$, however, and the propellant consumption and number of pulses also increase significantly (see ♦ labeled PPN, nav const. $= 3$).

Two additional PPN examples are considered in Fig. 11. Reference 8 develops a second-order Gaussian filter using a Cartesian state vector $[\underline{r}^T \ \ \underline{\dot{r}}^T]^T$ and relating it with the angle measurements through partial derivatives up to the second order. The performance of this filter using 25/10-ms pulses for two different values of $\underline{Q}$ with $\sigma_r^2 = 0.01$ and 0.001 in Eq. (25b) is shown in Fig. 11, wherein we observe that the miss distance, 1.1–1.2 cm, using a Gaussian filter is the same as the miss distance with the hybrid filters using PPN with 25/10 ms pulses and $\Phi(t_{go})$. The second-order Gaussian filter consumes more $\Delta \underline{V}$, however, than the best PPN scheme with the hybrid Kalman filter. Lastly, the miss distance for a reference case of the PPN guidance using true LOS rates and 25/10-ms pulses is ~1 mm, the smallest of all cases, with a higher ΔV consumption, as expected.

2. Predictive Guidance

Figure 11 considers five such schemes, labeled a–e ZEM: a) pulses of variable width $\tau_w \geq 10$ ms to null the estimated ZEM completely using the $4 \times 4\ \Phi_c$; b) pulses of variable width in the range 25 ms $\geq \tau_w \geq 10$ ms and the constant transition matrix Φ_c; c) pulses of width $\tau_w/2$ but still using Φ_c; d) pulses of width $\tau_w/2$ using the $4 \times 4\Phi(t_{go})$; and e) pulses of width $\tau_w/2$ using the 6×6 spherical transition matrix. In all of these cases, the pulse width is not shorter than 10 ms, and a pulse width longer than 25 ms, if demanded by guidance, is permitted. Case a, in which thrusters are fired each time for a complete duration of τ_w including $\tau_w > 25$ ms, uses excessive ΔV because of the ZEM estimation error, as one would expect. The total $\Delta \underline{V}$ drops significantly in case b when the pulse width is limited to 25 ms or shorter with the same constant transition matrix Φ_c. The miss distance of case b is about the same as the miss distance of case a, however. When thrusters are fired for only $\tau_w/2$ s (case c) instead of τ_w, additional propellant savings as well as shorter miss distances are realized. Because of shorter pulse width however, the number of pulses (not shown here) increases, as one would expect. As with the PPN, the miss distance for cases d and e are lower than the miss distance for the case c because of using the $\Phi(t_{go})$ transition matrix.

From the comparative results in Fig. 11, the conclusion emerges that if one employs the transition matrix $\Phi(t_{go})$ and the predictive guidance with $\tau_w/2$ pulses (case d) instead of full τ_w pulses, then the

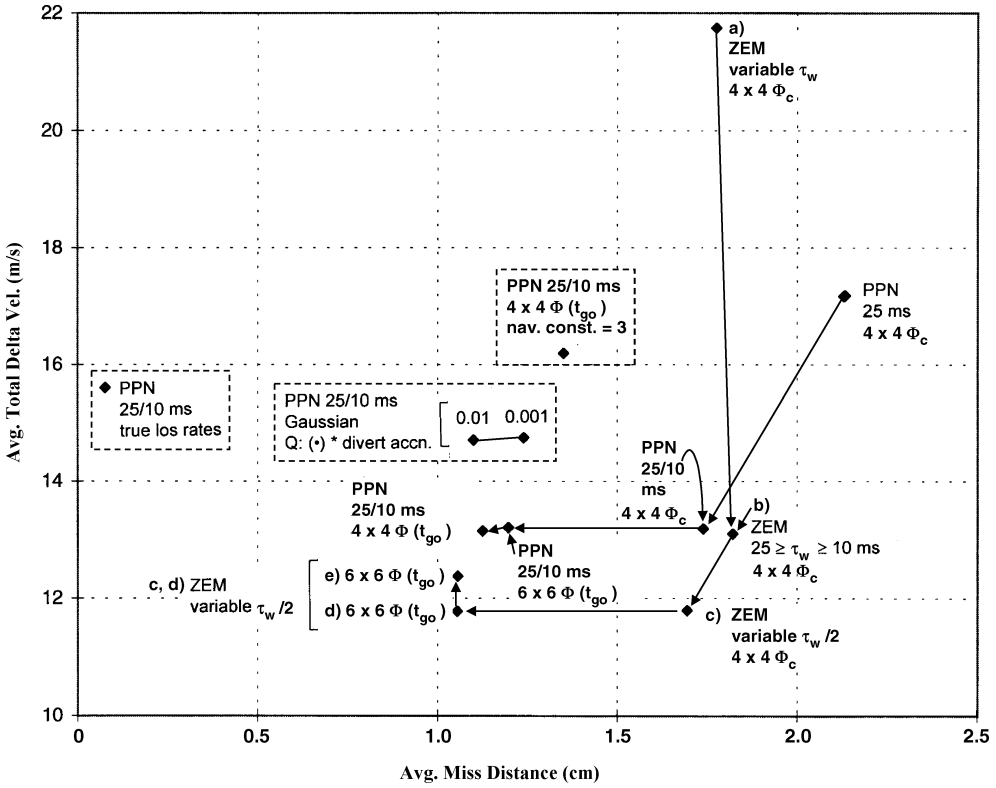

Fig. 11 Predictive guidance with the spherical transition matrix $\Phi(t_{go})$ yields smaller miss distance and lower divert requirement than the PPN guidance with the $\Phi(t_{go})$.

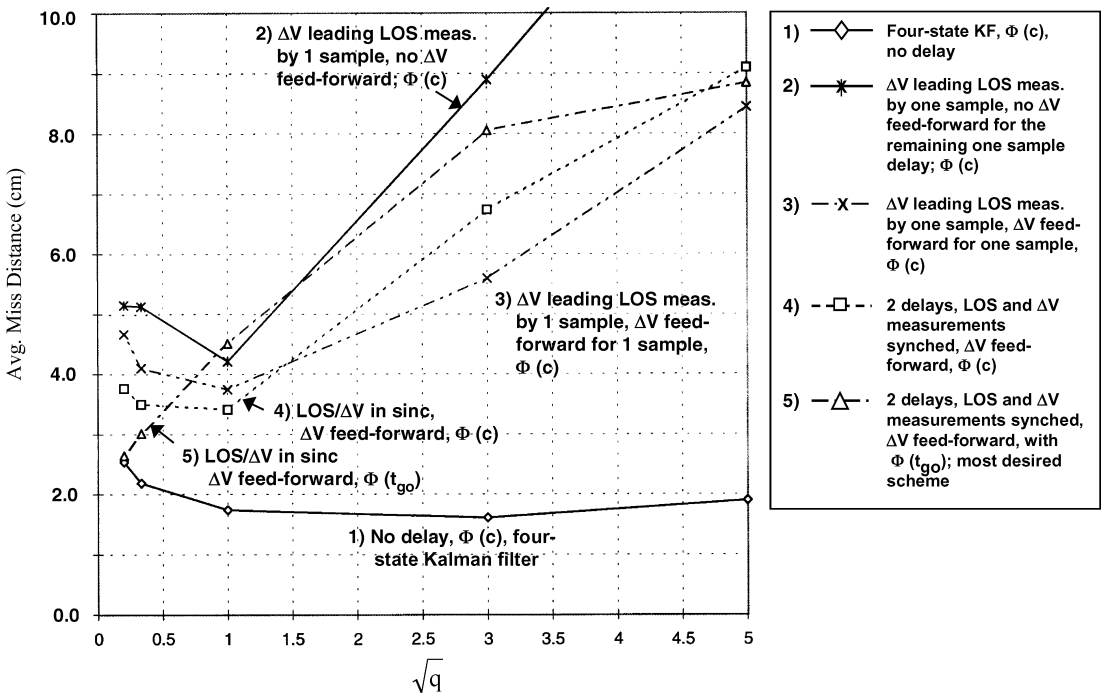

Fig. 12 Average miss distance vs $\sqrt{q}$ in the presence of one-sample LOS measurement delay and one-sample LOS rate estimate communication delay for guidance: four different schemes of LOS rate estimate feed forward.

predictive guidance achieves both shorter miss distance and lower ΔV than the best PPN guidance achieves using 25/10-ms pulses and $\Phi(t_{go})$. This conclusion is important because a lower ΔV reduces the interceptor weight, and fewer pulses result in a quieter, smoother focal plan operation.

E. Two-Sample Delay and Feed Forward of LOS Rate Estimates

We now illustrate the second objective of the paper: compensation of sensor processing delays with $\Delta \underline{V}$ feed forward (Fig. 5). The LOS measurement arrives for measurement update with a one-sample delay ($n_1 = 1$ in Fig. 6), and then the LOS rate estimate from the filter takes one additional sample period ($n_2 = 1$ in Fig. 6) to reach the guidance module where a divert thrust command is determined at the start of a sample period. The average miss distance vs $\sqrt{q}$ for five different cases is compared in Fig. 12, all using pulsed proportional navigation guidance, 25-ms pulse widths for all time, and either the 4×4 constant transition matrix Φ_c or the time-to-go dependent $\Phi(t_{go})$. The miss distances are averages of 650 runs as in Fig. 9.

Case 1 is the standard no-delay case depicted earlier in Fig. 3. We observe that the miss distance corresponding to $Q_{\text{nom}}(q=1)$ is essentially minimum, and therefore Q_{nom} is an appropriate nominal choice. Next, we consider case 2 in which the ΔV measurements are not stored to synchronize with the one-sample delayed seeker LOS measurement for update, and $\Delta \underline{V}$ is not fed forward to propagate the LOS rate estimates to compensate for the additional one frame delay. In other words, with reference to Fig. 5, the Kalman filter receives $\Delta \underline{V}_{k-1}$ instead of $\Delta \underline{V}_{k-2}$, and the velocity feed forward does not take place. The average miss distance vs $\sqrt{q}$ for this case (*) is shown in Fig. 12 and is the worst of all cases considered—the miss distance is the largest for each value of q except for $q=1$. This performance is improved step by step as follows.

Case 3 corresponds to the situation in which the hybrid Kalman filter still receives $\Delta \underline{V}_{k-1}$ instead of $\Delta \underline{V}_{k-2}$ as in case 2, but the one-sample delayed LOS rate estimate is propagated forward using $\Delta \underline{V}_{k-1}$. Figure 12 shows that this arrangement does decrease the miss distance, but the Kalman-filter formulation is still violated in that $\Delta \underline{V}_{k-1}$ over $t_{k-1} \le t \le t_k$ leads the LOS angle measurement θ_{k-1} by one sample. The performance is improved further in case 4, the □ curve, by synchronizing the $\Delta \underline{V}$ and the LOS measurements and including the $\Delta \underline{V}$ feed forward for the two-sample delay, in accordance with Fig. 5. As a result, relative to cases 2 and 3, the average miss distance drops for $Q \le Q_{\text{nom}}$.

Cases 1–3 use Φ_c to propagate the error covariance matrix P. For still further reduction of miss distance, Φ_c is replaced with $\Phi(t_{\text{go}})$ in case 5. This eliminates the accuracy mismatch in propagation of the state vector in Cartesian coordinates and of the error covariance matrix in spherical coordinates. The optimum Q matrix to achieve a smaller miss distance is now smaller than the previous optimum Q: For $\sqrt{q}=0.2$, the average miss distance decreases to 2.7 cm. Curiously, at Q_{nom} the miss distance with $\Phi(t_{\text{go}})$ is larger than the miss distance with Φ_c, implying that $Q=Q_{\text{nom}}$ is not optimal for $\Phi(t_{\text{go}})$. Indeed, when $\Phi(t_{\text{go}})$ is used, no modeling errors remain in the simulation, and, therefore, $Q=0$ is the optimum Q (no random process noise is simulated in these examples).

VII. Conclusions

The preceding study leads to the following conclusions. For a hybrid Kalman filter, a four-state time-to-go dependent spherical transition matrix yields essentially the same miss distance as a six-state spherical transition matrix, which estimates the target range. It is therefore adequate to use the four-state time-to-go dependent spherical transition matrix and process noise matrix for propagating the error covariance matrix for a hybrid Kalman filter. In the case of pulsed proportional navigation guidance, as the interceptor approaches a target the divert pulse duration should be shortened; otherwise, the miss distance will be overcorrected, and the interceptor will oscillate from one side of the target to the other instead of homing in exponentially. Whereas the predictive guidance, by definition, shortens the pulses progressively as the target is approached, the pulsed-proportional-navigation guidance does not. For this reason, the predictive guidance is superior to the pulsed proportional navigation guidance. However, for predictive guidance, as a result of the miss distance estimation errors, not all estimated miss distance should be eliminated in one firing. Instead, considerable propellant is saved if, say, half of the estimated miss distance is eliminated at a time. Then the predictive guidance achieves smaller miss distance, lower fuel consumption, and fewer divert firings than the proportional navigation guidance does. Adaptive, time-to-go dependent spherical state transition matrix and process noise matrix for propagating the spherical error covariance matrix in a hybrid Kalman filter lower the sensitivity of the miss distance to the hidden modeling errors. Finally, the delay in arrival of the line-of-sight measurements at the hybrid Kalman filter and in the communication of the line-of-sight rate estimates to the guidance module can be compensated for by synchronizing the incremental velocity measurements with the propagation of relative position and velocity before measurement update and with forward propagation of the delayed line-of-sight rate estimates over the delay period. The zero-delay miss distance and insensitivity to modeling errors are then almost restored.

References

[1]Zarchan, P., *Tactical and Strategic Missile Guidance*, 3rd ed., Progress in Astronautics and Aeronautics, Vol. 176, 1997, pp. 27, 28, 98, 155–161, 342–352; also Chaps. 23 and 24.

[2]Ben-Asher, J. Z., and Yaesh, I., *Advances in Missile Guidance Theory*, Progress in Astronautics and Aeronautics, Vol. 180, AIAA, Reston, VA, 1998, p. 2.

[3]Shneydor, N. A., *Missile Guidance and Pursuit: Kinematics, Dynamics and Control*, Horwood Publishing, Chichester, England, U.K., 1998, Sec. 6.3, pp. 131–140, and Appendix D.9, p. 242.

[4]Nesline, F. W., and Zarchan, P., "A New Lork at Classical vs Modern Homing Missile Guidance," *Journal of Guidance and Control*, Vol. 4, No. 1, 1981, pp. 78–85.

[5]Frankline, G. F., Powell, J. D., and Workman, M., *Digital Control of Dynamic Systems*, Addison Wesley Longman, 1997, Sec. 8.6.1, pp. 338–341.

[6]Mehra, R. K., "A Comparison of Several Nonlinear Filters for Reentry Vehicle Tracking," *IEEE Transactions on Automatic Control*, Vol. AC-16, No. 4, 1971, pp. 307–319.

[7]Grossman, W., "Bearings-Only Tracking: A Hybrid Coordinate System Approach," *Journal of Guidance, Control, and Dynamics*, Vol. 17, No. 3, 1994, pp. 451–457.

[8]Hablani, H. B., "Gaussian Second-Order Filter for Proportional Navigation of Exoatmospheric Interceptors with Angles-Only Measurements," *Proceedings of AIAA Guidance, Navigation, and Control Conference*, AIAA, Reston, VA, 1998, pp. 592–606.

[9]Stallard, D. V., "An Angle-Only Tracking Filter in Modified Spherical Coordinates," *Proceedings of AIAA Guidance, Navigation, and Control Conference*, AIAA, New York, 1987, pp. 542–550.

[10]Abzug, M. J., "Vector Methods in Homing Guidance," *Journal of Guidance and Control*, Vol. 2, No. 3, 1979, pp. 253–255.

[11]Rawling, A. G., "Passive Determination of Homing Time," *AIAA Journal*, Vol. 6, No. 8, 1968, pp. 1604–1606.

[12]Zarchan, P., and Musoff, H., *Fundamentals of Kalman Filtering*, Progress in Astronautics and Aeronautics, Vol. 190, AIAA, Reston, VA, 2000, Chap. 9, p. 355.

[13]Lawrence, R. V., "Advanced Missile Guidance," AIAA Paper 91-2726, Aug. 1991; also see AGARD Lecture Series 173, Paper 5, Sept. 1990.

[14]Barron, R. L., "Reduced-Computation End-Game Steering Laws for Predictive Guidance," *Journal of Guidance, Control, and Dynamics*, Vol. 18, No. 2, 1995, pp. 306–315.

[15]Lawrence, R. V., "Interceptor Line-of-Sight Rate Steering: Necessary Conditions for a Direct Hit," *Journal of Guidance, Control, and Dynamics*, Vol. 21, No. 3, 1998, pp. 471–476.

[16]Hablani, H. B., and Pearson, D. W., "Determination of Guidance Parameters of Exoatmospheric Interceptors via Miss Distance Error Analysis," AIAA Paper 2001-4279, Aug. 2001.

[17]Hablani, H. B., and Pearson, D. W., "Miss Distance Error Analysis of Exoatmospheric Interceptors," *Journal of Guidance, Control, and Dynamics*, Vol. 27, No. 2, 2004, pp. 283–289.

[18]Robinson, P. N., and Yin, M. R., "Modified Spherical Coordinates for Radar," *Proceedings of AIAA Guidance, Navigation, and Control Conference*, AIAA, Washington, DC, 1994, pp. 55–64.

[19]Nesline, F. W., and Zarchan, P., "Line-of-Sight Reconstruction for Faster Homing Guidance," *Journal of Guidance, Control, and Dynamics*, Vol. 8, No. 1, 1985, pp. 3–8.

[20]Allen, R. R., and Blackman, S. S., "Implementation of an Angle-Only Tracking Filter," *Signal and Data Processing of Small Targets*, edited by O. E. Drummond, Vol. 1481, Society of Photo-Optical Instrumentation Engineers, 1991, pp. 292–303.

[21]Bar-Shalom, Y., Rong Li, X., and Kirubarajan, T., *Estimation with Applications to Tracking and Navigation*, Wiley, New York, 2001, Secs. 6.2, 6.3, 11.2.